

An Unconventional Form of Actin in Protozoan Hemoflagellate, *Leishmania*^{*S}

Received for publication, January 9, 2008, and in revised form, May 12, 2008. Published, JBC Papers in Press, June 5, 2008, DOI 10.1074/jbc.M800213200

Prabodh Kapoor^{†1}, Amogh A. Sahasrabudhe[‡], Ashutosh Kumar^{†1}, Kalyan Mitra[§], Mohammad Imran Siddiqi[‡], and Chhitar M. Gupta^{‡2}

From the [†]Division of Molecular and Structural Biology and [§]Electron Microscopy Unit, Central Drug Research Institute, Lucknow-226001, India

Leishmania actin was cloned, overexpressed in baculovirus-insect cell system, and purified to homogeneity. The purified protein polymerized optimally in the presence of Mg²⁺ and ATP, but differed from conventional actins in its following properties: (i) it did not polymerize in the presence of Mg²⁺ alone, (ii) it polymerized in a restricted range of pH 7.0–8.5, (iii) its critical concentration for polymerization was found to be 3–4-fold lower than of muscle actin, (iv) it predominantly formed bundles rather than single filaments at pH 8.0, (v) it displayed considerably higher ATPase activity during polymerization, (vi) it did not inhibit DNase-I activity, and (vii) it did not bind the F-actin-binding toxin phalloidin or the actin polymerization disrupting agent Latrunculin B. Computational and molecular modeling studies revealed that the observed unconventional behavior of *Leishmania* actin is related to the diverged amino acid stretches in its sequence, which may lead to changes in the overall charge distribution on its solvent-exposed surface, ATP binding cleft, Mg²⁺ binding sites, and the hydrophobic loop that is involved in monomer-monomer interactions. Phylogenetically, it is related to ciliate actins, but to the best of our knowledge, no other actin with such unconventional properties has been reported to date. It is therefore suggested that actin in *Leishmania* may serve as a novel target for design of new antileishmanial drugs.

Trypanosomatid parasites of the genus *Leishmania* are the causative agents of several diseases ranging from relatively mild cutaneous lesions to disfiguring mucocutaneous manifestations and fatal visceral leishmaniasis, affecting millions of people worldwide (1). These organisms have a digenic lifecycle and exist in two morphologically distinct forms, *viz.* promastigotes and amastigotes. Whereas flagellated promastigote forms normally reside and divide in the alimentary tract of the sand fly

vector, aflagellated amastigote forms primarily exist within the phagolysosomal complex of the mammalian macrophages (2). The most characteristic structural feature of *Leishmania* parasites is their flagellar pocket, which is bound by the membrane network devoid of microtubules, and is the only site that is engaged in endocytotic and exocytotic processes (3, 4). These processes in the trypanosomatids are essentially required not only for nutrient uptake but also in evasion of host defense (5). It has recently been shown that depletion of the cytoskeleton protein, actin, in the bloodstream form of *Trypanosoma brucei* inhibited endocytosis that subsequently resulted in cell death, suggesting that actin is indispensable during this process (6).

Actin is a ubiquitous cytoskeleton protein in eukaryotes, which exists in monomeric (G-actin) and filamentous (F-actin) forms and plays an important role in several vital cellular processes such as cell motility, cell division, endocytosis, intracellular trafficking, etc. (7). Although this protein is well characterized in a number of organisms including protozoans, like *Entamoeba* (8), *Tetrahymena* (9, 10), *Paramecium* (11), *Dictyostelium* (12), *Plasmodium* (13, 14), and *Toxoplasma* (15), little is known about the biochemical properties and cellular functions of actin present in trypanosomatid parasites, such as *Leishmania* and *Trypanosoma* (6, 16). However, it has recently been shown by immunolabeling techniques that actin in *Leishmania*, besides being present in cortical regions and the flagellar pocket, is also present in the kinetoplast and nucleus, where it appeared to co-localize with DNA (16, 17). We therefore, envisage that actin in *Leishmania* may also be involved in other cellular processes such as chromatin/k-DNA remodeling (18).

Earlier attempts to isolate *Leishmania/Trypanosoma* actin by using a conventional method of DNase-I affinity chromatography were unsuccessful, as this enzyme did not bind to trypanosomatid actin in whole cell lysates (19). Also, staining with fluorescently labeled phalloidin failed to stain filamentous actin in these organisms (16, 19, 20). Moreover, no filament-like structures corresponding to mammalian actin filaments (5–7 nm diameter) could be visualized by using electron microscopy (20, 21). Based on these observations, it was believed that actin may play only a limited role in cellular activities of trypanosomatid parasites, and that this protein is perhaps not a major cytoskeleton protein in these organisms (20–22). However, recent work from our laboratory has shown that *Leishmania* contains abundant quantities of actin, which is mainly present in the form of granules, patches, and filament-like structures (16). It has further been shown that these filament-like struc-

* This work was supported in part by a research grant from CDRI and the Department of Biotechnology, Government of India, New Delhi (India) under the Distinguished Biotechnologist Award Scheme (to C. M. G.). This is communication 7446 from CDRI. The costs of publication of this article were defrayed in part by the payment of page charges. This article must therefore be hereby marked "advertisement" in accordance with 18 U.S.C. Section 1734 solely to indicate this fact.

[§] The on-line version of this article (available at <http://www.jbc.org>) contains supplemental Figs. S1 and S2.

[†] Recipients of research fellowships from the Council of Scientific and Industrial Research, Rafi Marg, New Delhi (India).

² To whom correspondence should be addressed: Chhitar Manzil Palace, M G Rd., Central Drug Research Institute, Lucknow-226001, India. Fax: 91-522-2623405; E-mail: drcmg@sify.com.

tures are associated with an F-actin-binding protein, coronin (23).

To fully characterize the biochemical properties of *Leishmania* actin (LdACT),³ we have now overexpressed this protein in the baculovirus-insect cell expression system, purified it to homogeneity, and compared its biochemical properties with the purified rabbit muscle actin (RbACT). Comparative biochemical analysis of the purified protein revealed that LdACT markedly differed from RbACT in its various properties that distinguish LdACT as a novel form of eukaryotic actin.

EXPERIMENTAL PROCEDURES

Cell Culture

Sf9 insect cells (Invitrogen) were maintained at 27 °C as monolayer cultures in TNM-FH medium (Invitrogen). These cells were routinely subcultured at 3–4-day intervals and were replaced with frozen stocks after every 3 months. The *Leishmania donovani* strain (DD8) was obtained from the National Institute of Immunology, New Delhi (India), and maintained in high glucose Dulbecco's modified Eagle's nutrient medium, supplemented with 10% fetal bovine serum and 40 mg/liter gentamycin at 25 °C. pENTR/SD/D-TOPO as a baculovirus entry vector was procured from Invitrogen, whereas p6.5 as an episomal expression vector was a kind gift from Prof. K. P. Chang (University of Chicago, Chicago, IL).

Antibodies

Monospecific, polyclonal antibodies to *Leishmania* actin (LdACT) and coronin (LdCORO) were raised in rabbits and mice, respectively, and purified using published procedures (16, 23). Purified anti-recombinant LdACT and anti-LdCORO antibodies specifically recognized only LdACT and LdCORO, respectively, in the whole cell lysates of *Leishmania* promastigotes. Antibodies against α , β -tubulins (monoclonals) were procured from ICN, antibodies against GRP78 was a kind gift from Dr. E. Handman, and fluorophore-tagged IgGs were purchased from Molecular Probes.

Plasmid Construction, Transfection, and Expression

Expression of LdACT in the Baculovirus-Insect Cell System—Genomic DNA from cultured *L. donovani* promastigotes was isolated using standard protocol (24). For insect cell transfection, the coding sequence of LdACT was PCR amplified using primers 5'-CACCATGGCTGACAACGAGCAGAGCTCCATCG-3' (forward) and 5'-CTCGAGTTAGTGGTGGTGGTGGTGGAAACACTTGTATGCACGATGCTCGGCC-3' (reverse), which incorporated sequence coding for the His₆ tag at the C terminus of the protein, and genomic DNA as the template. The PCR product was subsequently cloned into viral transfer vector pENTR/SD/D-TOPO and sequenced by the dideoxy chain termination method (25). Entry vector containing LdACT was subjected to *in vitro* LR

recombination with linearized baculodirect genomic DNA at 25 °C (Invitrogen). Recombinant viruses were obtained after 96 h by transfection of LR recombination product into Sf9 cells in the presence of 100 μ M ganciclovir as per the manufacturer's instructions. Transfected Sf9 cells were assayed 96 h postinfection for the expression of LdACT-His₆ (rLdACT) by 10% SDS-PAGE and Western blot analysis using mouse monoclonal antibodies against hexahistidine (Amersham Biosciences) as well as rabbit monospecific polyclonal antibodies against LdACT, followed by HRP-conjugated goat anti-mouse IgG/anti-rabbit IgG. Signals were captured by chemiluminescence detection (Millipore) and exposure to x-ray film.

Homologous Expression of LdACT in *Leishmania Promastigotes*—Episomal expression of LdACT in *L. donovani* promastigotes was made possible by a homologous episomal expression vector p6.5. The construct p6.5-LdACT was generated by PCR amplification of LdACT using primers 5'-GCTAGCATGGCTGACAACGAACAGAGCTCC-3' (forward) and 5'-AAGCTTTCAGAAGCACTTGTATGCACGATGCT-3' (reverse) and genomic DNA as the template, and the PCR product was subsequently cloned in p6.5 vector at NheI and HindIII sites (present in the vector multiple cloning site, and forward and reverse primers respectively). The presence of LdACT in the construct was examined by restriction enzyme digestion and the nucleotide sequence was confirmed by DNA sequencing using the dideoxy chain termination method (25). 40 μ g of both the p6.5-LdACT construct and p6.5 control plasmids were transfected separately into 10⁷ *L. donovani* promastigotes by electroporation (26). Transfected cells were further selected in the growth medium containing tunicamycin up to 20 μ g/ml and maintained in the same conditions. Lysates of both p6.5-LdACT- and p6.5-transfected promastigotes prepared by lysing equal number of cells were separated by 10% SDS-PAGE, transblotted onto polyvinylidene fluoride membrane, washed, and blocked, as described previously (16, 23), and probed with rabbit anti-LdACT antibodies as well as mice anti-GRP78 antibodies (protein loading control) followed by HRP-conjugated goat anti-mouse IgG and anti-rabbit IgG. Signals were captured by chemiluminescence detection and exposure to x-ray film. Band intensities were determined by densitometric analysis. The level of LdACT expression in transfected promastigotes was cross-confirmed by flow cytometry. For this, both p6.5-LdACT- and p6.5-transfected promastigotes (10⁶ cells) were harvested, washed two times with phosphate-buffered saline, fixed with 4% paraformaldehyde, permeabilized with 0.1% Triton X-100 containing 0.5% glycine, and suspended in phosphate-buffered saline. Cells were then treated with rabbit anti-LdACT antibodies, followed by fluorescein isothiocyanate-conjugated anti-rabbit IgG, and analyzed by using a FACS Calibur (BD Biosciences) flow cytometer using Cell Quest support software for acquisition and analysis.

Purification of Proteins

All the purification steps were performed in cold below 20 °C. Sf9 cells infected with recombinant baculovirus (multiplicity of infection 0.8) were harvested at 72 h postinfection and lysed in 1 M Tris-HCl, pH 7.5, 0.6 M KCl, 0.5 mM Na₂ATP, 1 mM dithiothreitol and protease inhibitors containing 0.5 mM 4-(2-

³ The abbreviations used are: LdACT, *Leishmania* actin; RbACT, rabbit actin; TRITC, tetramethylrhodamine B isothiocyanate; HRP, horseradish peroxidase; C_c, critical concentration; MOPS, 4-morpholinepropanesulfonic acid; MES, 4-morpholineethanesulfonic acid; Ni²⁺-NTA, nickel-nitrilotriacetic acid.

Unconventional Actin in *Leishmania*

aminoethyl)benzenesulfonyl fluoride hydrochloride, 5 mM benzamidine hydrochloride, 5 $\mu\text{g/ml}$ leupeptin, 1 $\mu\text{g/ml}$ E64, and 10 $\mu\text{g/ml}$ N^α -tosyl-L-lysine chloromethyl ketone hydrochloride. Cells lysate was clarified and dialyzed overnight into 15 mM MOPS, pH 7.0, 0.2 mM CaCl_2 , 0.2 mM dithiothreitol, 0.25 mM Na_2ATP , and 1 $\mu\text{g/ml}$ leupeptin. Lysate was then passed through a SP Sepharose column (Amersham Biosciences) two times and flow through was dialyzed into G-buffer (5 mM Tris-HCl, pH 8.2, 0.2 mM CaCl_2 , 0.2 mM dithiothreitol, and 0.25 mM Na_2ATP). After dialysis it was incubated with Ni^{2+} -NTA-agarose beads for 1 h, preequilibrated with G-buffer. Beads were washed with G-buffer containing 20 mM imidazole, and rLdACT was eluted with G-buffer containing 200 mM imidazole. The eluted fraction was concentrated with an Amicon Ultracentrifugal filter device (Millipore) and finally purified on a Superdex 75 HR 10/300 column on AKTA fast performance liquid chromatography (GE Healthcare). The peak fraction was tested for purity by 12% SDS-PAGE and was found to be about 95% pure. Purified rLdACT thus obtained was utilized within 2–3 days for further experiments. Rabbit skeletal muscle actin was purified from rabbit muscle acetone powder as described by Pardee and Spudich (27) and stored in lyophilized form at -80°C after addition of sucrose (2 mg/mg protein). RbACT was subjected to size exclusion chromatography using a Superdex 75 HR 10/300 column on AKTA fast performance liquid chromatography each time after thawing a new frozen vial, and only the peak fractions of monomeric actin were used in the experiments.

Actin Polymerization

Sedimentation Assay—Actin polymerization was monitored by ultracentrifugation as reported earlier (28). Purified rLdACT or RbACT was first incubated in G-buffer for 1 h on ice followed by ultracentrifugation at $100,000 \times g$ for 20 min at 4°C to remove traces of aggregates, if any. In the supernatant fractions, actin polymerization was initiated by adding 1/10th volume of $\times 10$ F-actin buffer to make the final concentration of 0.1 M KCl, 2 mM MgCl_2 , and 2 mM ATP and incubated at 25°C for another 2 h. Although the concentration of ATP used was higher, but ATP in this range has been used earlier for the polymerization of conventional as well as various homologs of actin, without any adverse effect on actin (15, 29). Samples were centrifuged at $140,000 \times g$ at 25°C for 2 h. Pellet fractions were washed once with F-actin buffer, resolved on 10% SDS-PAGE, and stained with Coomassie Brilliant Blue R-250 or transblotted onto polyvinylidene fluoride membrane and probed with rabbit anti-LdACT antibodies followed by HRP-conjugated goat anti-rabbit IgG and chemiluminescence detection.

Fluorescence Quenching and Light Scattering Assay—Actin polymerization was also monitored by measuring the decrease in intrinsic tryptophan fluorescence as reported earlier (30). Intrinsic tryptophan fluorescence emission spectra for actin samples were obtained on a PerkinElmer LS50B Spectroluminescence meter in a 5-mm path length quartz cell. Samples were excited with 290 nm and their respective emissions were scanned from 300 to 500 nm. Actin polymerization was monitored by adding 1/10th volume of $\times 10$ F-actin buffer to the solution containing varying concentrations of protein followed

by incubation at 25°C for 2 h. The critical concentration was determined by plotting the change in fluorescence after adding F-actin buffer to different concentrations of rLdACT or RbACT. The time course of actin polymerization was monitored by recording light scattering at 90° from the axis of incident light of 400 nm wavelength (excitation slit width 1.5 nm, emission slit width 2.5 nm) as described previously (31) using an RF-540 spectrofluorimeter.

DNase-I Inhibition and TRITC-Phalloidin Binding

DNase-I inhibition assay was performed in the presence of rLdACT and RbACT as described earlier (32). Briefly, 10 μl of DNase-I (4 μM) was added to samples containing a range of protein concentrations in G-buffer and incubated for 30 min at 25°C . Salmon sperm DNA (6 μl of 10 mg/ml) was added to each sample prior to recording the absorbance at 260 nm in a Shimadzu UV-1650 PC Spectrophotometer. Linear rates of hyperchromicity were monitored for DNase-I activity and plotted in terms of % inhibition of DNase-I activity with increasing concentrations of actin. Additionally, the effect of rLdACT and RbACT on the activity of DNase-I was also compared by adding both the actins separately to the reaction mixture containing DNase-I and salmon sperm DNA followed by agarose gel electrophoresis, as described earlier (33). For this, 100 ng of bovine pancreatic DNase-I (Fermentas) was preincubated with 2 μg /reaction of G-actin (rLdACT or RbACT) in DNase-I buffer (10 mM Tris-HCl, pH 8.0, 4 mM MgCl_2 , 4 mM CaCl_2) for 30 min at room temperature, followed by addition of 3 μg /reaction of salmon sperm DNA and the samples were incubated at room temperature for another 45 min. To terminate the reaction, 25 mM EDTA was added to each reaction and the samples were resolved on a 1% agarose gel and photographed under UV light. Binding of phalloidin with F-actin on the other hand was analyzed using an earlier published procedure (28). Briefly, rLdACT or RbACT over a range of protein concentrations were polymerized separately in F-actin buffer for 2 h at room temperature. After polymerization, F-actin in each sample was labeled with 2 μM TRITC-phalloidin (sigma) and the increase in fluorescence of TRITC-phalloidin was monitored by measuring fluorescence (λ_{em} 585 nm, λ_{ex} 544 nm) on a PerkinElmer LS50B Spectroluminescence meter. Additionally, binding of the phalloidin to both rLdACT and RbACT was also analyzed by measuring the decrease in tryptophan fluorescence of polymerized actin upon binding with phalloidin. For this, 2 μM rLdACT and RbACT with various replicates were polymerized separately in F-actin buffer at 25°C for 2 h. After polymerization, increasing concentrations of the ligand (TRITC-phalloidin) were added and the samples were further incubated at 25°C for 30 min. Finally, samples were analyzed for their respective tryptophan fluorescence on a PerkinElmer LS50B Spectroluminescence meter (λ_{em} 300–500 nm, λ_{ex} 290 nm).

Immunofluorescence Microscopy

Leishmania promastigotes and infected Sf9 cells were fixed with 4% (w/v) paraformaldehyde in 200 mM HEPES buffer (pH 7.2) at 25°C for 30 min, and washed two times for 5 min each with phosphate-buffered saline containing 0.5% (w/v) glycine. The washed cells were allowed to adhere on the poly-L-lysine-

coated coverslips. Fixed cells were permeabilized with 0.1% (v/v) Triton X-100 and blocked with 10% (v/v) goat serum (Amersham Biosciences) in phosphate-buffered saline for 30 min. After blocking, the cells were first incubated with primary antibodies (10 $\mu\text{g}/\text{ml}$) at 4 °C and then stained with Oregon Green and/or Texas Red-X-tagged secondary antibodies (10 $\mu\text{g}/\text{ml}$) at 4 °C for 4 h in the dark. Coverslips were mounted in the mounting medium (Oncogene) and images were collected using a $\times 63$, 1.4 NA (oil) Plan Apochromate lens on a Leica DM5000B fluorescence microscope. Green and red images were collected separately after excitation at 488 and 543 nm, respectively, and merged for presentation.

Electron Microscopy

rLdACT and RbACT were polymerized separately in F-actin buffer at 25 °C for 2 h. For each specimen, 6 μl of the samples were allowed to adsorb for 2 min on a freshly glow-coated carbon-coated copper grid (300 mesh). After blotting off the excess fluid from the grid, staining was done with 1% aqueous uranyl acetate solution. Finally, grids were air dried and observed under a FEI Tecnai-12 Twin Transmission Electron Microscope equipped with a SIS MegaView II CCD camera at 120 kV. Measurements were done using AnalySIS software (SIS, Herzogenrath, Germany).

ATP Hydrolysis and Inorganic Phosphate Release Assay

ATP hydrolysis by RbACT and rLdACT during their polymerization was monitored by using the malachite green assay as described earlier (34). Polymerization of both RbACT and rLdACT was initiated separately by the addition of $\times 10$ F-actin buffer at 25 °C. At 2-min intervals, the reaction was deproteinized with 1 volume of cold 0.6 M perchloric acid and stored on ice until all samples for the different time points were collected. The samples were centrifuged and their supernatants were removed for inorganic phosphate determination. To each sample 1/4th volume of coloring agent (0.44 g of malachite green, 3% (w/v) ammonium molybdate, 0.2 ml of 11% Tween 20 in 2.6 N H_2SO_4) was added, incubated at room temperature for 30 min, and absorbance measured at 630 nm using a precision microplate reader. The curves were normalized with KH_2PO_4 standard and a control without protein. P_i produced *versus* time was plotted for various concentrations of both the actins. The rate of P_i produced at the linear part of each curve was determined and plotted as a function of actin concentration to determine the rate of ATP hydrolysis presented in terms of P_i produced ($\mu\text{M}/\text{min}$).

Release of inorganic phosphate during polymerization of RbACT and rLdACT was determined with the EnzChek kit (Molecular Probes) employing a procedure modified from the manufacturer's instructions because of significant absorbance of light at 360 nm by polymerized RbACT and rLdACT. Parallel reactions were carried out with and without the EnzChek enzyme and reactant components. Both reactions were read in real time at 360 nm in a Shimadzu UV-1650 PC Spectrophotometer. Polymerization of both RbACT and rLdACT were initiated by the addition of $\times 10$ F-actin buffer at 25 °C and the absorbance of RbACT and rLdACT alone were subtracted from those of the complete reactions. A standard curve of P_i concen-

trations was employed as per the manufacturer's instructions. Phosphate release curves were overlain onto the 400-nm light scattering curves of parallel polymerization reactions carried out in the RF-540 spectrofluorimeter. The completion phase of each curve was set to 100% and the values of each curve were normalized with the 100% value.

Circular Dichroism Measurements

Ellipticity spectra were recorded between 200 and 250 nm in a Jasco J810 spectropolarimeter calibrated with ammonium (+)-10-camphorsulfonate. The values obtained were normalized by subtracting the baseline recorded for the buffer having the same concentration of the constituent ions under similar conditions and the results were expressed as mean residual ellipticity. Thermal denaturation was monitored by change in molar ellipticity at 222 nm as a function of temperature on the same spectropolarimeter, equipped with a peltier temperature controller system. Samples were heated at constant rate of 1 °C/min in a 1-mm path length cell.

Phylogenetic Analysis, Homology Modeling, and Molecular Dynamics Simulations

The amino acid sequences of actin from various organisms, *viz.* *Amoeba proteus* (gi 33946363), *Dictyostelium discoideum* (gi 113218), *Saccharomyces cerevisiae* (gi 38372623), *Paramecium caudatum* (gi 15212111), *Tetrahymena thermophila* (gi 84344), *Cryptosporidium cohnii* (gi 19908693), *Lingulodinium polyedrum* (gi 37694465), *Toxoplasma gondii* (gi 606857), *Plasmodium falciparum* (ACT1, gi 160053), *Cryptosporidium parvum* (gi 113293), *Cryptosporidium hominis* (gi 54657132), *Perkinsus marinus* (gi 38112716), *Arabidopsis thaliana* (gi 30687201), *Caenorhabditis elegans* (gi 6626), *Drosophila melanogaster* (gi 156773), *Homo sapiens* (β -actin, gi 4501885), *H. sapiens* (γ -actin, gi:28339), *Trypanosoma brucei* (gi 71755105), and *Leishmania donovani* (gi:28627572) were aligned using ClustalW software (35) and the alignment was saved in Phylip format. Phylogenetic relationships of LdACT with actins from various organisms were inferred from the PHYLIP package (version 3.66) (36). Bootstraps were obtained with the SEQBOOT program (1000 data sets were generated) and distance matrices were generated with the PRODIST program (Jones-Taylor-Thornton matrix). Neighbor-joining analysis was carried out with the NEIGHBOR program using the input order of sequences. Phylogenetic trees were drawn with TreeIllustrator software (37). The three-dimensional model of the *L. donovani* actin monomer was built based on four actin crystal structure templates *Oryzactolagus cuniculus*, Protein Data bank code 2A5X (38); *C. elegans*, PDB code 1D4X (39); *S. cerevisiae*, PDB code 1YAG (39); and *D. discoideum*, PDB code 1NM1 (39) using Modeler program interfaced with InsightII 2000.1 (40). Subsequently, the model was energetically minimized with 500 steps of steepest descent minimization, followed by 2000 steps of conjugate gradient minimization to remove the geometrical strain. To further investigate the ATP binding with *L. donovani* actin, the ATP was manually docked to the binding site based on the previous structural information (41).

This initial binary complex structure was further refined by energy minimization. To examine the ATP-induced conforma-

Unconventional Actin in *Leishmania*

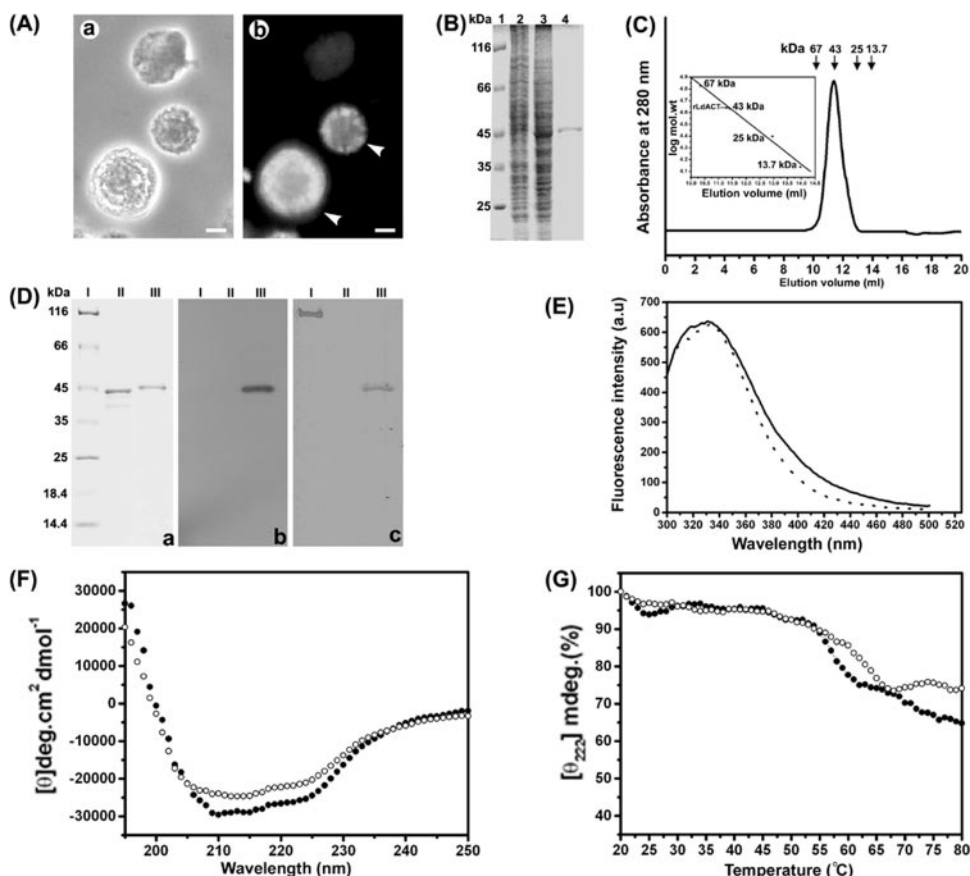


FIGURE 1. Expression, purification, and biophysical characterization of rLdACT. *A*, expression of rLdACT in Sf9 cells after 72 h post-infection with recombinant baculovirus, (*a*) phase, and (*b*) fluorescence image of infected Sf9 cells stained with rabbit anti-rLdACT antibodies followed by fluorescein isothiocyanate-conjugated anti-rabbit IgG. Bar, 5 μ m. *B*, Coomassie-stained SDS-polyacrylamide gel electrophoretic analysis of recombinant *L. donovani* actin (rLdACT) overexpressed in Sf9 cells. Lane 1, molecular weight markers; lane 2, uninfected Sf9 cells; lane 3, Sf9 cells after 72 h post-infection with recombinant baculovirus; lane 4, eluate after Ni²⁺-NTA chromatography containing purified rLdACT. *C*, size exclusion profile of the rLdACT after Ni²⁺-NTA chromatography showing the monomeric nature of purified rLdACT and only the peak fractions were used in further experiments. Arrows mark peak positions of the marker proteins: albumin (67 kDa), ovalbumin (43 kDa), chymotrypsinogen (25 kDa), ribonuclease A (13.7 kDa). Inset shows the apparent molecular mass of the purified rLdACT to be 43 kDa. *D*, molecular identity of rLdACT by Western blot analysis; *a*, Coomassie-stained gel; lane I, molecular weight markers; lane II, purified rabbit muscle actin (RbACT); lane III, purified rLdACT. *b*, Western blot developed using rabbit anti-rLdACT antibodies followed by HRP-conjugated anti-rabbit IgG, which detected only rLdACT (lane III) in the blot and not RbACT (lane II). *c*, blot was stripped off and the same blot was developed after probing it with mice anti-His₆ monoclonal antibody followed by HRP-conjugated anti-mice IgG, which detected rLdACT (lane III) as well as the molecular mass marker of 116 kDa (lane I) that also contained a His₆ tag (positive control). *E*, fluorescence emission spectra of rLdACT (solid line) and RbACT (dotted line). *F*, far UV CD spectra of rLdACT (filled circles) and RbACT (open circles). *G*, thermal unfolding of rLdACT (filled circles) and RbACT (open circles) in terms of percentage ellipticity plotted versus temperature.

tional changes in *L. donovani* actin, two independent 500-ps MD simulations in the presence and absence of ATP were carried out with the CHARMM program using CHARMM force field (42). All *L. donovani* actin systems were solvated using Explicit Spherical Boundary with harmonic restraints (sphere of 50 Å radius). This solvated complex was subjected to energy minimization first by 500 steps of steepest descent followed by 2000 steps of conjugate gradient method. The system was heated from 50 to 300 K over a period of 50 ps with a time step of 1 fs and the velocities being reassigned in the system every 0.05 ps. The system was further equilibrated with a 1-fs time step, for 100 ps so that the energy of the system achieves complete stability. Production runs were performed at 300 K and carried out under a constant number of particles, volume, and temperature conditions for 500 ps with a 1-fs time step. All the

bonds involving hydrogen atom were constrained using the SHAKE algorithm in all simulations (43). The molecular trajectory for the systems generated by the molecular dynamics simulations were analyzed using the VMD (44) software and the CHARMM program (42).

RESULTS

Cloning, Overexpression, and Purification of rLdACT

Several attempts were made to purify native LdACT, or recombinant protein using the yeast expression system, but without any success. However, we could successfully purify this protein in its properly folded form by expressing it in the baculovirus-insect cell expression system. A hexahistidine tag was attached to the C terminus of LdACT to facilitate the purification process, because earlier studies have shown that the presence of the His₆ tag at the N or C terminus of actins has no significant effect on their polymerization properties (15, 45, 46). LdACT with a C-terminal His₆ tag was cloned under control of the polyhedron promoter of baculovirus and the presence of LdACT-His₆ in the viral genome was confirmed by PCR (data not shown). LdACT-His₆ was subsequently expressed in Sf9 insect cells as a recombinant protein (rLdACT) that accumulated in the cytosol of host cells, as shown by SDS-PAGE analysis of the lysate as well as by fluorescence imaging of 72 h post-infected Sf9 cells (Fig. 1, *A* and *B*). rLdACT was purified from infected Sf9 cells harvested at 72 h postinfection with subsequent

ion exchange, Ni²⁺-NTA, and size exclusion chromatography and only monomeric peak fractions were used for further experiments (Fig. 1, *B*-*D*). Structural integrity of the purified rLdACT was established by comparing its tryptophan fluorescence (Fig. 1*E*) spectra and far UV-CD (Fig. 1*F*) spectra with that of RbACT. To rule out the possibility of partial unfolding of rLdACT during purification, we measured the unfolding kinetics of rLdACT and RbACT under identical conditions; both rLdACT and RbACT unfolded approximately with the same rates (0.2514 and 0.2307 min⁻¹, respectively) when their thermal denaturation was monitored in the same transition zone (50–65 °C) (Fig. 1*G*).

Properties of rLdACT

rLdACT Differs from RbACT in Its Polymerization Conditions— Polymerization of both rLdACT and RbACT was monitored

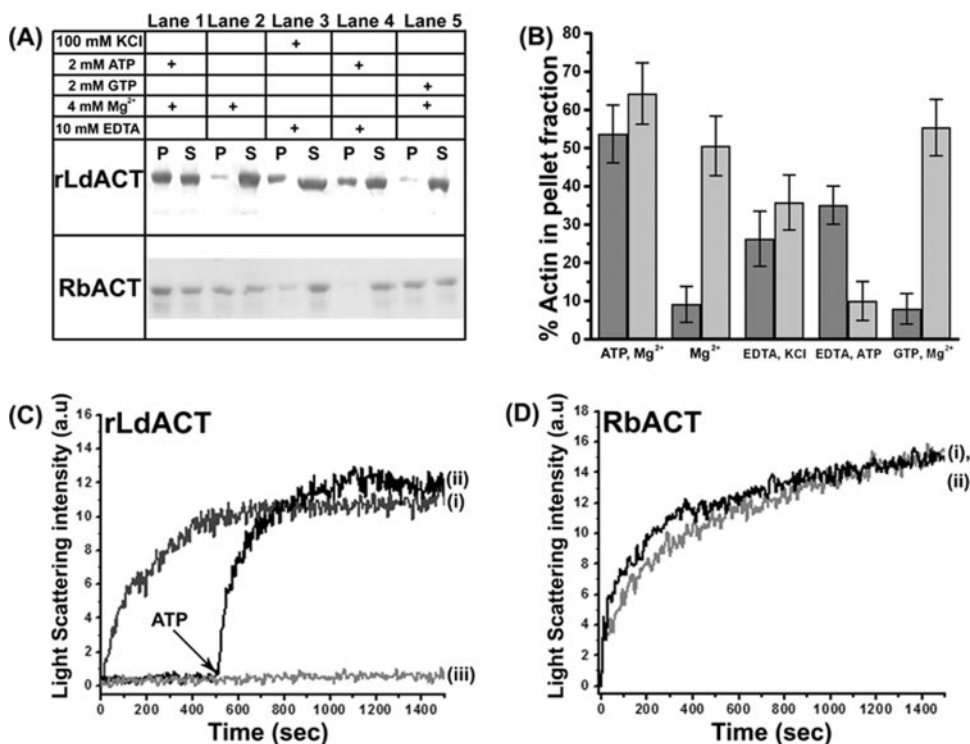


FIGURE 2. Polymerization properties of rLdACT and RbACT assessed by pelleting and 90° light scattering assay. *A*, Coomassie-stained SDS-polyacrylamide gel of rLdACT and RbACT under different ionic or nucleotide conditions after centrifugation at $140,000 \times g$. *P*, actin in pellet fraction, and *S*, actin in supernatant fraction. Both the actins were used at the concentration of $5 \mu\text{M}$. *B*, bar graph representing percentage of actins in pellet fractions. *Dark gray bars*, rLdACT; *light gray bars*, RbACT, values shown are mean of three independent experiments \pm S.D. *C*, light scattering measurements of $5 \mu\text{M}$ rLdACT in the presence of (i) 2 mM Mg²⁺ and 2 mM ATP, (ii) 2 mM Mg²⁺ followed by 2 mM ATP supplementation after 500 s (marked by arrow), and (iii) 2 mM Mg²⁺. *D*, light scattering measurements of $5 \mu\text{M}$ RbACT in the presence of (i) 2 mM Mg²⁺ and 2 mM ATP, (ii) 2 mM Mg²⁺.

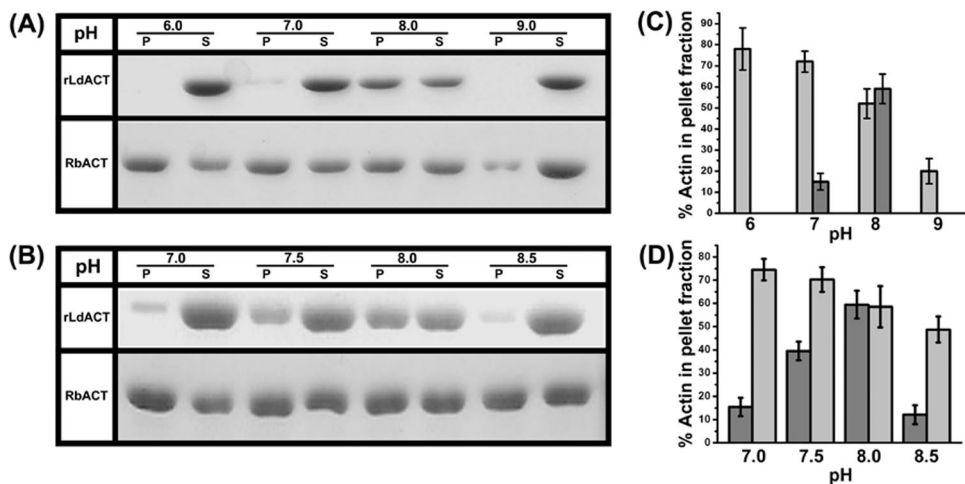


FIGURE 3. pH-dependent polymerization of rLdACT. *A* and *B*, Coomassie-stained SDS-polyacrylamide gel electrophoretic analysis of LdACT and RbACT, after their polymerization at different pH values and centrifugation at $140,000 \times g$. *P*, actin in pellet fraction, and *S*, actin in supernatant fraction. Both actins were used at a concentration of $5 \mu\text{M}$. *C* and *D*, bar graph representing the percentage of actins in pellet fractions of rLdACT and RbACT. *Dark gray bars*, rLdACT; *light gray bars*, RbACT, values shown are mean of three independent experiments \pm S.D. Buffers at pH (i) 6.0 (MES), (ii) 7.0 (HEPES), (iii) 8.0 (Tris), and (iv) 9.0 (Tris) were used for polymerization.

under various conditions by both pelleting and light scattering assay. Although maximum polymerization of both rLdACT and RbACT was observed when ATP was used along with Mg²⁺, rLdACT unlike RbACT, underwent polymerization even in the complete absence of any divalent cation (Fig. 2, A

and *B*). Moreover, very little, if any, polymerization of rLdACT was seen when Mg²⁺ alone or Mg²⁺ with GTP were used in the polymerization medium, whereas considerable polymerization of RbACT was observed under these conditions, suggesting higher preference of rLdACT for ATP as a nucleotide and that Mg²⁺ alone in the polymerization buffer is not sufficient enough to induce polymerization of rLdACT. These observations further gain strength when the time course of polymerization of both rLdACT and RbACT was monitored in the presence of Mg²⁺ alone and in combination with ATP (Fig. 2, *C* and *D*). A significant increase in light scattering intensity was observed when polymerization of RbACT was monitored in the presence of Mg²⁺ alone, whereas no light scattering intensity enhancement was observed under similar conditions with rLdACT. To rule out the possibility of denaturation of rLdACT in the absence of ATP, polymerization up to the first 500 s was monitored in the presence of only Mg²⁺, which revealed no increase in light scattering intensity suggesting insignificant polymerization, however, after the first 500 s, when ATP was supplemented in the same reaction mixture, a significant increase in light scattering intensity was observed that followed the same time course of polymerization as in the presence of ATP and Mg²⁺ (Fig. 2*C*), thus suggesting ATP as an essential component for the polymerization of rLdACT. The possibility of structural alterations in rLdACT in the presence of Mg²⁺ alone was further eliminated by measuring its tryptophan fluorescence and far UV CD spectra in the presence of the Mg²⁺ (supplemental Fig. S1). It may be noted that a major part of both actins was found to be in supernatant fractions. To rule out the possibility of some amount of denatured protein in

these fractions, we analyzed the structural integrity of the supernatant protein that was found to be unchanged (data not shown). It may therefore be envisaged that the actins remaining in the supernatant may exist in the form of short filaments that could not be sedimented at the measured speed of centrifuga-

Unconventional Actin in *Leishmania*

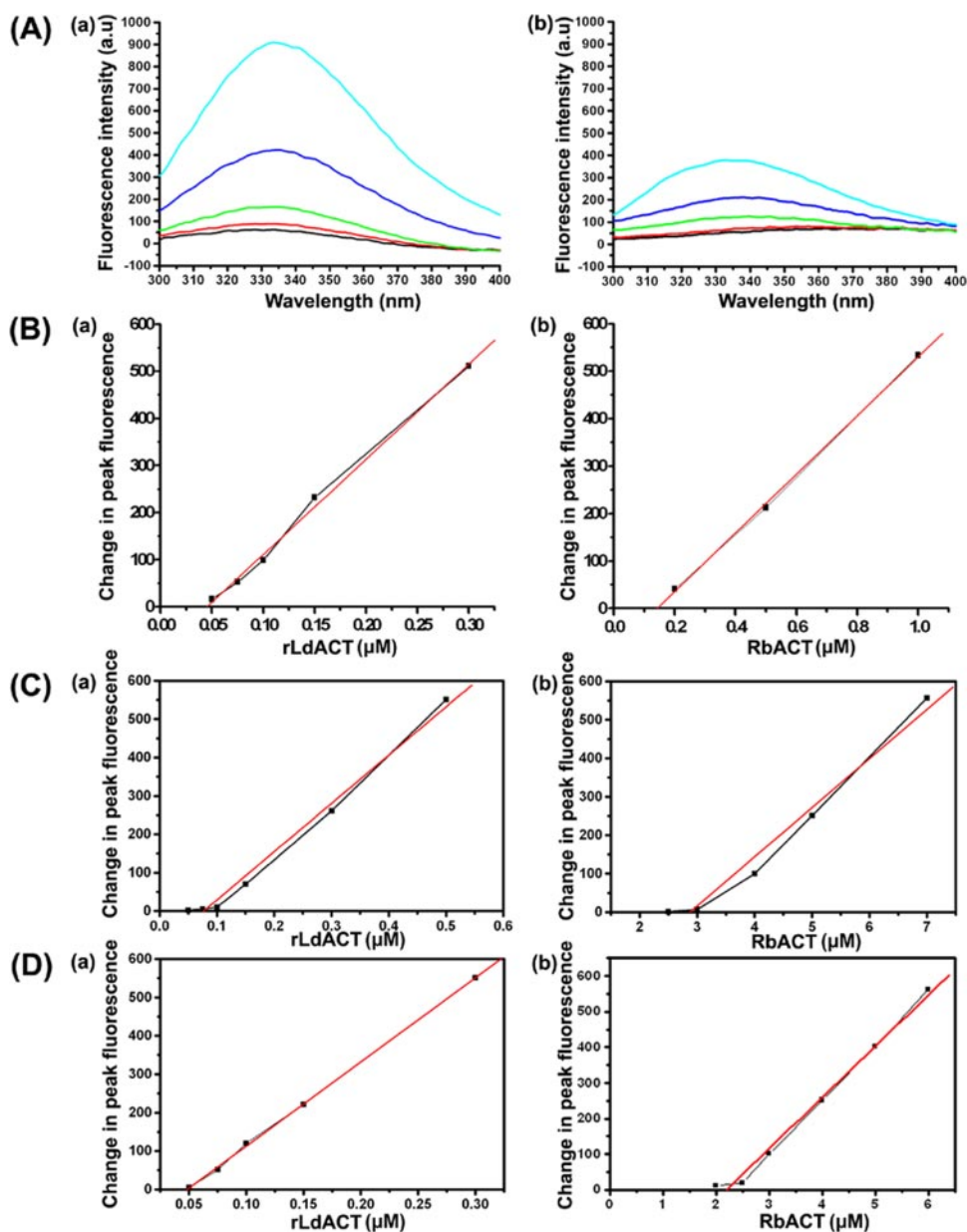


FIGURE 4. Critical concentration determination of rLdACT. *A*, tryptophan fluorescence quenching curves of rLdACT at its different concentrations (μM) in G-buffer (*a*) and F-buffer (*b*). Measurements were made 2 h after addition of F-buffer. *B*, (*a*) plot of change in tryptophan peak fluorescence between G-buffer and F-buffer as a function of the rLdACT concentration revealed the C_c of rLdACT to be $\sim 0.04 \mu\text{M}$, (*b*) plot of change in the tryptophan peak fluorescence between G-buffer and F-buffer as a function of RbACT concentration, which revealed the C_c of RbACT to be $\sim 0.16 \mu\text{M}$. *C*, (*a*) C_c of rLdACT in the presence of $5 \mu\text{M}$ cytochalasin D, (*b*) C_c of RbACT in presence of $5 \mu\text{M}$ cytochalasin D. *D*, (*a*) C_c of rLdACT in presence of $5 \mu\text{M}$ Latrunculin B, (*b*) C_c of RbACT in presence of $5 \mu\text{M}$ Latrunculin B.

tion. This apart, polymerization of rLdACT occurred in a narrow range of pH from 7.0 to 8.5 and no polymerization was observed when pH of the medium was <7.0 , however, RbACT was observed to polymerize in a broad pH range with maximum polymerization at pH 6.0 (Fig. 3).

Critical Concentration (C_c) for Polymerization of rLdACT Is Significantly Lower Than of Conventional Actin—Polymerization of rLdACT and RbACT at varying concentrations was monitored by measuring the quenching of their intrinsic tryptophan fluorescence after addition of F-actin buffer (Fig. 4A). This was based on the earlier studies that showed that intrinsic tryptophan fluorescence is quenched when G-actin is con-

verted into F-actin under *in vitro* conditions (30). Upon plotting the change in tryptophan fluorescence as a function of monomeric actin concentration, the C_c of rLdACT and RbACT were calculated around 0.04 and $0.16 \mu\text{M}$, respectively (Fig. 4B). This was further validated by monitoring actin polymerization by the sedimentation assay, which showed a linear increase in amounts of actin in the pellet fractions with increasing rLdACT concentrations above $0.04 \mu\text{M}$ (data not shown). Based on the earlier observations that cytochalasin D inhibits polymerization at the barbed ends and thereby polymerization occurs only at the pointed ends (47), we determined the C_c of rLdACT and RbACT in the presence of $5 \mu\text{M}$ cytochalasin D. C_c of both RbACT and rLdACT increased to 2.9 and $0.08 \mu\text{M}$, respectively (Fig. 4C). Latrunculin B has earlier been shown to interact with actin in 1:1 stoichiometry and affect its C_c (48). We, therefore, determined the C_c of rLdACT and RbACT in the presence of $5 \mu\text{M}$ Latrunculin B. Whereas the C_c of RbACT was altered to $2.4 \mu\text{M}$, the C_c of rLdACT remained unaffected (Fig. 4D), suggesting that Latrunculin B does not affect the polymerization of rLdACT under *in vitro* conditions.

rLdACT Predominantly Assembles in the Form of Bundles at pH 8.0—rLdACT and RbACT were polymerized *in vitro* at various concentrations under identical conditions, and the polymers thus formed were analyzed by electron microscopy. Unlike RbACT (Fig. 5A, panel *a*), rLdACT at the concentration of $2 \mu\text{M}$ existed largely in the form of

bundles (Fig. 5A, panel *b*), however, when the concentration of rLdACT in the polymerization mixture was lowered to $0.2 \mu\text{M}$ and the pH of the F-actin buffer was brought down from 8.0 to 7.0, besides forming bundles, it also existed in the form of filaments (Fig. 5A, panel *c*). The average diameter of these *in vitro* assembled rLdACT filaments was found to be around 5 nm , which was well within the range of the diameter of *in vitro* assembled filaments of other eukaryotic actins ($5\text{--}7 \text{ nm}$).

Homologous Expression of LdACT in *Leishmania* Reveals Long Cables of Actin—Earlier studies from our laboratory have shown that actin is abundantly present in *Leishmania*, which mainly exists in the form of granules, patches, and filament-like

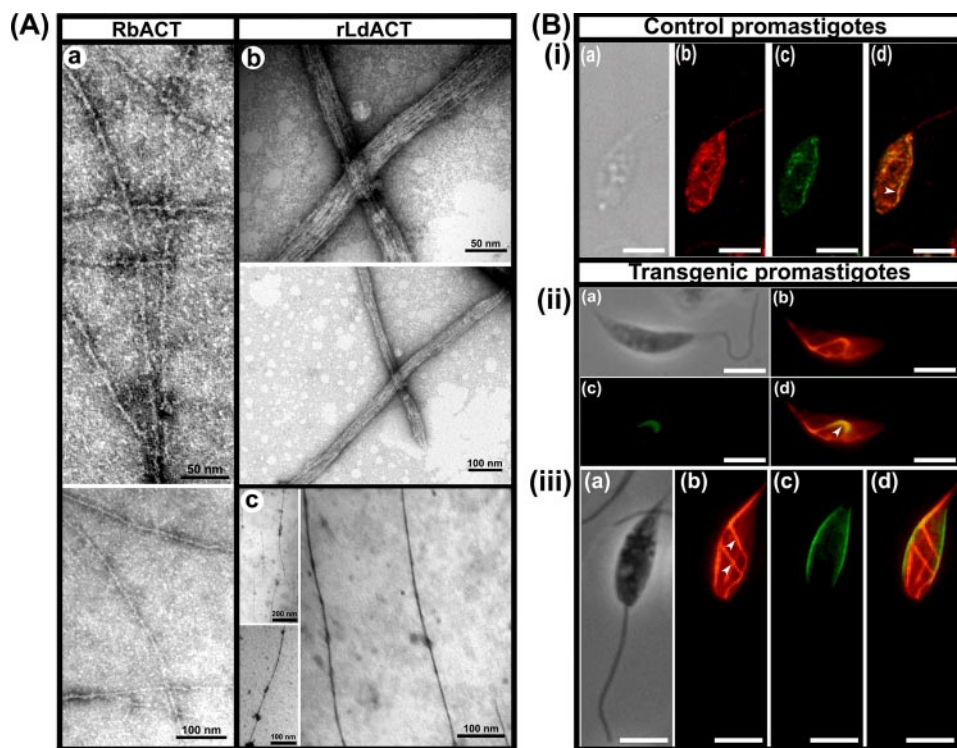


FIGURE 5. *In vitro* and *in vivo* analysis of LdACT filaments. *A*, *a*, electron microscopic images of *in vitro* constituted RbACT filaments in F-buffer (pH 8.0) at 2 μM protein concentration. *b*, electron microscopic images of *in vitro* polymerized rLdACT filaments under identical buffer conditions, pH 8.0, and protein concentration (2 μM) as in RbACT, which revealed the existence of rLdACT filaments primarily in the form of bundles. *c*, to visualize isolated filaments rLdACT was polymerized at a concentration of 0.2 μM and the pH of F-buffer was lowered to 7.0. Under these conditions, RbACT does not form well defined filaments. *B*, immunofluorescence imaging of control and transgenic promastigotes. (i) control promastigotes: (a) phase, (b) labeled with anti-LdACT antibodies (red), (c) labeled with anti-LdCORO antibodies (green), and (d) merge of b and c. Arrowhead shows colocalization of actin filaments with coronin in the control promastigotes. (ii) transgenic promastigotes: (a) phase, (b) labeled with anti-LdACT antibodies (red), (c) labeled with anti-LdCORO antibodies (green), and (d) merge of b and c. Arrowhead shows colocalization of almost the entire endogenous F-actin-binding protein, coronin, with bundles of LdACT filaments. (iii) transgenic promastigotes: (a) phase, (b) labeled with anti-LdACT antibodies (red), (c) labeled with anti-tubulin antibodies (green), and (d) merge of b and c. Arrowhead shows bundles of actin filaments in the transgenic promastigotes. Bar, 5 μm .

structures (16). It was further shown that the filament-like structures of actin are invariably associated with an actin-binding protein, coronin (23). To analyze whether overexpression of actin in *Leishmania* cells would increase the occurrence of its filamentous form in these cells, we episomally overexpressed LdACT in *L. donovani* promastigotes and then analyzed the status of actin. The levels of actin expression in *Leishmania* cells that were transfected with the p6.5-LdACT construct (transgenic cells) were compared with the cells that were transfected with the vector alone (control cells) by Western blot analysis, using GRP78 as the internal protein control (supplemental Fig. S2B) as well as by flow cytometry (supplemental Fig. S2C). The levels of actin in the transgenic cells were 3–4 times greater than that in the control parasites. To examine the status of actin in these cells, we immunostained both the transgenic and control cells with anti-LdACT, anti-LdCORO, and anti- α,β -tubulin antibodies and then analyzed the stained cells with immunofluorescence microscopy (Fig. 5B). LdACT in transgenic parasites was predominantly present in the form of long filaments that largely existed as cables, whereas in control cells it was present as granules, patches, and short filaments. Interestingly, most of the actin filaments and cables seen in the transgenic cells, like the control cells were found to be deco-

rated with endogenous coronin, further confirming the ability of coronin to invariably associate with filamentous actin in *Leishmania* cells.

rLdACT Exhibits Higher ATPase Activity and Fast P_i Release during Its Polymerization—Hydrolysis of tightly bound ATP in actin filaments (F-ATP actin \leftrightarrow F-ADP- P_i actin) followed by the release of P_i to form F-ADP actin is a characteristic property of all eukaryotic actins during their polymerization. The intermediate F-ADP- P_i actin thus formed assures stability of the filaments, whereas P_i release from the complex has been shown to be an elementary step responsible for the weakening of the monomer-monomer interactions within the filaments (49, 50). Because amino acid sequence alignment of five ATP-binding motifs (two adenosine ring binding and three phosphate binding) in LdACT with ATP-binding motifs of other eukaryotic actins (51) revealed a high degree of divergence in motif 3 of LdACT that binds the adenosine ring, we determined the effect of this difference on ATP hydrolysis. P_i release as well as ATP hydrolysis during polymerization of both rLdACT and RbACT were monitored following the

standard procedure (31). rLdACT was found to assemble with a much higher rate of P_i release as a consequence of higher ATP hydrolysis as compared with RbACT (Fig. 6).

rLdACT Does Not Inhibit DNase-I Activity—All eukaryotic actins are known to bind DNase-I and inhibit its activity with the exception of *Entamoeba* and *Tetrahymena* actins (8, 9). Because the DNase-I binding loop in LdACT is highly diverged as compared with mammalian actins (16), we compared the effects of rLdACT and RbACT on the activity of DNase-I. Although RbACT inhibited DNase-I activity up to 97% even at low concentrations, rLdACT did not affect DNase-I activity at all (Fig. 7A) under identical conditions. This was further confirmed by agarose gel electrophoresis of salmon sperm DNA digested with DNase-I in the presence or absence of rLdACT or RbACT. Fig. 7B shows that DNase-I incubated with rLdACT completely hydrolyzed salmon sperm DNA (lane 4), similar to control DNase-I without any actin (lane 2). However, DNase-I did not hydrolyze salmon sperm DNA when rLdACT was replaced with RbACT in the incubation mixture (lane 5), demonstrating the inability of rLdACT to inhibit DNase-I activity. The possibility of intrinsic endonucleolytic activity in the purified protein was eliminated by incubating salmon sperm DNA with rLdACT and RbACT separately (Fig. 7B, lanes 6 and 7).

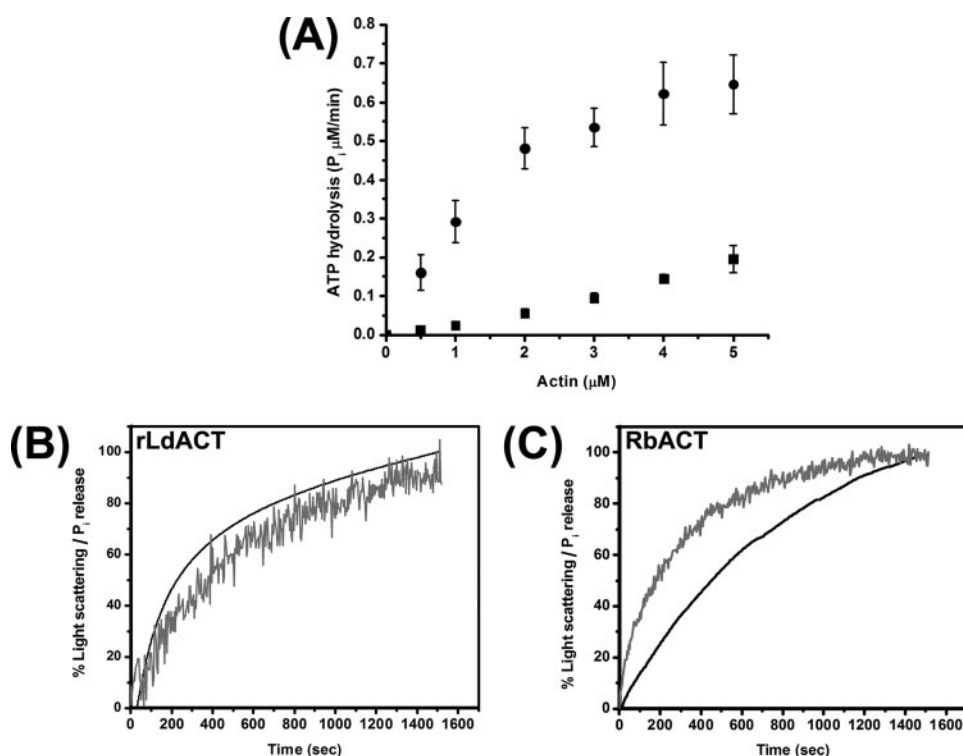
Unconventional Actin in *Leishmania*

FIGURE 6. ATP hydrolysis and P_i release during the course of polymerization of rLdACT and RbACT. A, plot showing comparison of the rate of ATP hydrolysis during *in vitro* polymerization of varying concentrations of rLdACT (filled circles) and RbACT (filled squares) under identical conditions. Measurements were made up to 30 min after addition of F-buffer using the malachite green assay as described under "Experimental Procedures." P_i produced versus time were plotted for various concentrations of both the actins. The rate of P_i produced at the linear part of each curve was determined and plotted as a function of actin concentration to determine the rate of ATP hydrolysis presented in terms of P_i produced (μ M/min). Values shown are mean of three independent experiments \pm S.D. for each concentration of both the actins. B and C, time-dependent P_i release (black lines) during polymerization of 5 μ M rLdACT, compared with 5 μ M RbACT, respectively. Measurements were done using EnzChek kit as described under "Experimental Procedures" and the kinetics of P_i release of rLdACT and RbACT were overlaid with their respective polymerization curve (gray lines) measured separately under identical conditions in a RF-540 spectrofluorimeter. The completion phase of each curve was set to 100% and the values of each curve were normalized with the 100% value.

TRITC-Phalloidin Does Not Bind rLdACT Filaments—TRITC-phalloidin, a fluorescently labeled bicyclic peptide, binds and stabilizes actin filaments *in vitro* and microfilaments inside the cell (7). Although we have already reported the inability of fluorescently labeled phalloidin to stain filament-like structures of actin in *Leishmania* (16), it was not clear whether *Leishmania* actin failed to bind phalloidin due to some conformational alterations in its structure or the observed inability was merely due to the *in situ* masking of phalloidin-binding sites by some actin-binding proteins. To address this, we compared the binding of TRITC-phalloidin with *in vitro* polymerized rLdACT and RbACT by measuring the enhancement in fluorescence of TRITC-phalloidin at 585 nm after incubating it with varying concentrations of polymerized actins. Fig. 7C shows that unlike RbACT, rLdACT did not show any enhancement of fluorescence even at 4 μ M rLdACT concentration, suggesting that rLdACT filaments have no affinity for TRITC-phalloidin at the measured concentrations. To rule out the possibility of failure of fluorescence enhancement of TRITC-phalloidin upon binding with rLdACT filaments due to the intrinsic nature of rLdACT, we measured the tryptophan fluorescence of polymerized rLdACT and RbACT after addition of increasing concentrations of phalloidin.

As a matter of fact, binding of phalloidin to actin filaments should decrease its tryptophan fluorescence intensity at 340 nm, which was observed with RbACT, however, polymerized rLdACT did not show any significant decrease in its fluorescence intensity at 340 nm even at higher concentrations of phalloidin (Fig. 7, D and E), thus showing the inability of rLdACT filaments to bind TRITC-phalloidin. Similar lack of phalloidin binding has earlier been reported only with *Tetrahymena* actin (9).

Phylogenetic Analysis

Although, the primary amino acid sequence of LdACT is \sim 70% identical to other eukaryotic/conventional actins, key residue differences could bring diversity in the overall structure that might be responsible for its unconventional behavior. LdACT showed high divergence in a few amino acid residues, *viz.* 1–9, 40–53, 194–200, 229–240, 266–281, and 307–315, that have been found to be conserved in mammalian actins. These differences in LdACT were phylogenetically analyzed with respect to the sequences of other available eukaryotic actins. A dendrogram based on neighbor-joining analysis was generated by comparing various available actin sequences from different organisms including LdACT using the PHYLIP program and robust tree topologies thus obtained were found to be in agreement with previously known taxonomic classifications. Fig. 8 shows the neighbor-joining analysis tree obtained with 1000 bootstrap replicates. The resulting phylogenetic tree exhibited a major cluster involving trypanosomatid actins and ciliate actins. These results clearly suggest that despite a high level of identity to eukaryotic/conventional actins, key differences are conserved among LdACT and ciliate actins.

comparing various available actin sequences from different organisms including LdACT using the PHYLIP program and robust tree topologies thus obtained were found to be in agreement with previously known taxonomic classifications. Fig. 8 shows the neighbor-joining analysis tree obtained with 1000 bootstrap replicates. The resulting phylogenetic tree exhibited a major cluster involving trypanosomatid actins and ciliate actins. These results clearly suggest that despite a high level of identity to eukaryotic/conventional actins, key differences are conserved among LdACT and ciliate actins.

Homology Modeling and Molecular Dynamics Simulation

Highly unconventional biochemical properties of LdACT observed here strongly suggest that LdACT may significantly differ from other eukaryotic actins in its three-dimensional structure. To evaluate this possibility, we developed an *in silico* energetically minimized model of LdACT using computational modeling along with molecular dynamic simulations. A three-dimensional model of *L. donovani* actin monomer, based on four crystal structure templates of actin (*O. cuniculus*, PDB code 2A5X; *C. elegans*, PDB code 1D4X; *S. cerevisiae*, PDB code 1YAG; *D. discoideum*, PDB code 1NM1) was generated and subsequently subjected to energy

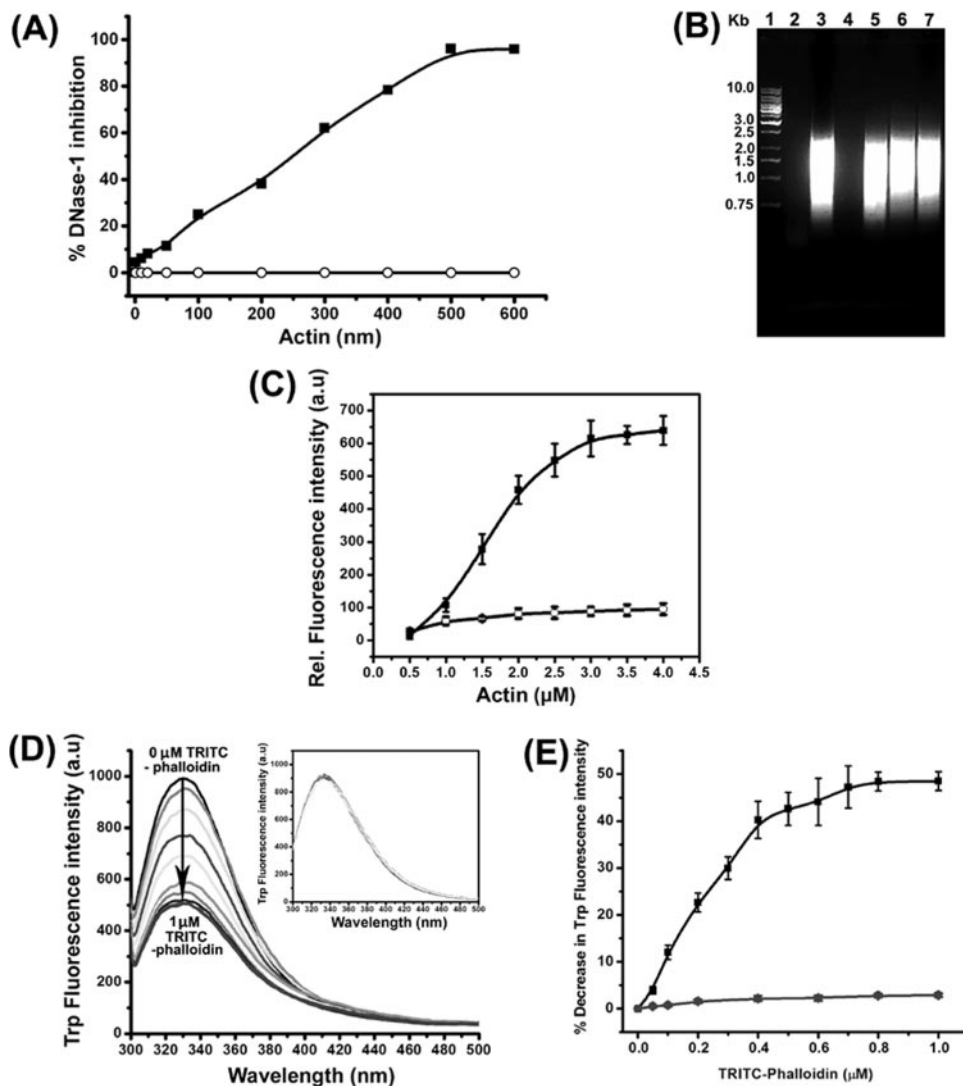


FIGURE 7. DNase-I inhibition activity and TRITC-phalloidin binding of rLdACT and RbACT. DNase-I inhibition assay: *A*, plot showing percentage of pancreatic DNase-I (100 nM) inhibition by increasing concentrations of monomeric RbACT (filled squares) and rLdACT (open circles) in the solution; *B*, agarose gel electrophoresis of salmon sperm DNA digested with pancreatic DNase-I in the presence or absence of monomeric rLdACT or RbACT. Lane 1, 1-kb DNA ladder; lane 2, 100 ng of DNase-I + 3 μ g of salmon sperm DNA (+ve control); lane 3, 3 μ g of salmon sperm DNA (-ve control); lane 4, 100 ng of DNase-I + 2 μ g of rLdACT + 3 μ g of salmon sperm DNA; lane 5, 100 ng of DNase-I + 2 μ g RbACT + 3 μ g of salmon sperm DNA; lane 6, 2 μ g of rLdACT + 3 μ g of salmon sperm DNA; lane 7, 2 μ g of RbACT + 3 μ g of salmon sperm DNA. *C*, plot showing fluorescence intensity of 2 μ M TRITC-phalloidin after incubating with increasing concentrations of polymerized rLdACT (open circles) and RbACT (filled squares), values shown are mean of three independent experiments \pm S.D. *D*, tryptophan fluorescence spectra of polymerized RbACT and rLdACT (inset) at 2 μ M protein concentration after incubating with increasing concentrations of TRITC-phalloidin. *E*, plot showing a comparison of the percent decrease in tryptophan fluorescence intensity of polymerized RbACT (solid squares) and rLdACT (solid circles) with increasing concentrations of TRITC-phalloidin, which shows no affinity of polymerized rLdACT with TRITC-phalloidin. Values shown are mean of three independent experiments \pm S.D.

minimization and molecular dynamics simulation in the presence or absence of ATP as described under "Experimental Procedures." All the key diverged amino acid residues were found to be concentrated on the surface of the monomer, especially including those regions that participate in filament formation, like DNase-I loop (Fig. 9A). However, interestingly this loop showed similar high fluctuations throughout the simulation (Fig. 9B), as found in the simulations with other conventional actins (52), suggesting the retention of overall flexibility in the DNase-I loop even after high diversity. Moreover, apart from the DNase-I loop a

region in subdomain 4 also showed marked fluctuations as revealed by average root mean square fluctuations values, indicating the retention of flexible regions involved in filament formation. However, diverse residues could alter interactions within the filaments or between the filaments or both, which could be better explained after exploring the structures of LdACT filaments. As revealed by the atomic structure of the actin·DNase-I complex (41), the major contacts between actin and DNase-I involved residues Gly⁴², Val⁴³, and Met⁴⁴ of actin, which are replaced by Met, Gln, and Ala, respectively, in LdACT, thereby making LdACT unable to inhibit DNase-I activity. Moreover, in the same atomic structure Thr²⁰³, Glu²⁰⁷, and Lys⁶¹ have been shown to form weak electrostatic interactions with DNase-I, which were conserved in LdACT (Fig. 9A), suggesting the prime importance of the major interactions in DNase-I inhibition by actin. Divergence in the key residues also brought about a high variation in the solvent-exposed surface charges in LdACT (Fig. 10A). Additionally, subdomain 2 was observed to be more closer to subdomain 4 (10.447 Å) compared with rabbit actin (13.872 Å), which led to structural alterations in the ATP-binding cleft resulting in the smaller cleft volume as compared with rabbit actin (Fig. 10A).

ATP binding cleft in LdACT is formed by residues Gly¹⁴, Ser¹⁵, Gly¹⁶, Met¹⁷, Lys¹⁹, Gln¹³⁸, Asp¹⁵⁵, Asp¹⁵⁸, Lys²¹⁴, Glu²¹⁵, Gly³⁰³, Ser³⁰⁴, Met³⁰⁶, Phe³⁰⁷, and Lys³³⁷ and lies between the lobes formed by subdomains 1 and 2 and subdomains 3 and 4 (Fig. 10B). These residues were consistent with the earlier reported residues for ATP binding with rabbit actin (41). To further understand how the ATP binding site reorganized itself upon binding of ATP, we compared the side chain orientations of the LdACT and the binary complex (with ATP). Among the residues that interacted with ATP, Lys¹⁹ showed the most dramatic conformational change. In the initial "apo" structure, Lys¹⁹ pointed away from the ATP binding site, but in our molecular dynamics simulations of the apoprotein, Lys¹⁹ showed considerable flexibility and changed orientation often. In the binary complex

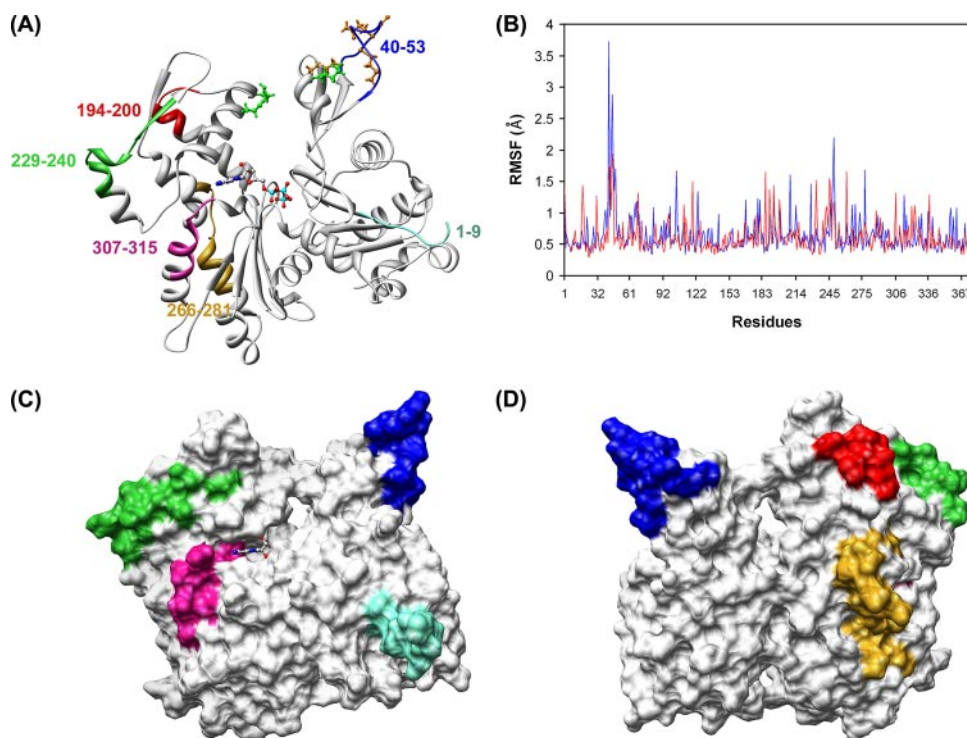


FIGURE 9. Computational modeling. *A*, average model of LdACT after molecular dynamic simulations showing colored stretches of diverged amino acid residues (1–9 in subdomain 1, 40–53 in subdomain 2, 266–281 and 307–315 in subdomain 3, 194–200 and 229–240 in subdomain 4), *brown ball and stick* residues in the DNase-I binding loop are the diverged replacements in LdACT that are known to make strong interactions with DNase-I in the actin-DNase-I complex crystal structure, whereas *green ball and stick* residues are conserved amino acid residues that are known to make weak interactions with DNase-I. *B*, graph showing root mean square fluctuations (measured in Å) as a function of amino acid residues observed throughout the trajectory of MD simulation analysis, *red*, without ATP; and *blue*, with ATP. *C* and *D* are the opposite faces of LdACT average model showing distribution of diverged amino acid residues throughout the surface of the molecule.

interaction of ATP in the ATP binding cleft at low pH may weaken the interactions between ATP and actin, which in turn may not promote actin polymerization.

The intracellular pH in both *Leishmania* promastigotes and amastigotes is maintained at around 7.0 to 7.5 by the highly efficient proton pumps present in their plasma membrane (59), despite the presence of *Leishmania* amastigotes within the phagolysosomal compartment of the host macrophages where they encounter very low pH (<5.0). Therefore, pH sensitivity of actin polymerization should not pose any problem within the parasites. This is well supported by the presence of filament-like actin structures in wild type *Leishmania* promastigotes and actin cables in actin overexpressing transgenic promastigotes. As a matter of fact, pH sensitivity of actin is perhaps to the advantage of the parasite, because it may be exploited to efficiently regulate the actin dynamics by fine regulation of the intracellular pH.

The C_c of LdACT was about 3–4-fold lower than of conventional actins and the resulting filaments largely existed in the form of bundles, suggesting that monomer-monomer interactions within and between the filaments in LdACT may be different than in the RbACT. It has earlier been proposed that the hydrophobic loop (amino acid residues 266–274) in the conventional actins between subdomains 3 and 4 extended away from the monomers and inserted into the hydrophobic pocket formed by the interface of two monomers in the opposing strands of the actin double helix (60). Interestingly, this loop is absent in the bacterial homologs of actin, MreB and ParM, resulting in diverged

structures of their filaments (61). The loop is highly diverged in the case of LdACT (amino acid residues 266–281), which may perhaps be responsible for its tendency to polymerize at relatively low concentrations and also to form bundles due to altered monomer-monomer interactions between the two strands of LdACT filaments. Alternatively, differences in surface charge distribution between LdACT and RbACT may be responsible for the bundling property of LdACT filaments. Actin bundling has recently been shown to play an important role in endocytosis (62). Interestingly, depletion of actin in the bloodstream form of *T. brucei* focused its role during endocytosis, which is an indispensable process for the survival of the parasites (6). It is therefore likely that the bundling property of actin may have been required by these parasites during endocytosis. Furthermore, C_c of LdACT in the presence of 5 μM cytochalasin D, which decreases the polymerization at the barbed ends but still allows assembly at the pointed ends, is increased to 0.08

μM , suggesting that the mechanism underlying the assembly of LdACT monomers into bundles may be similar to that reported earlier for conventional actins (47).

ATP hydrolysis during the polymerization of actin and subsequent release of P_i is the major factor in regulation of filament stability (50). This property is conserved from prokaryotic homologs of actin to all eukaryotic actins (45, 49). In most of the eukaryotic actins release of P_i lags the polymerization, whereas with the yeast actin it has been shown to be virtually instantaneous (63). During polymerization of LdACT, ATP hydrolysis was found to be higher. In the absence of a well defined catalytic mechanism of ATP hydrolysis during actin polymerization, it has been postulated that ATP hydrolysis involves a relatively closed state conformation of the actin superfamily members bringing the terminal phosphate of ATP in contact with the catalytic residues that are believed to be present in the first major domain (64). Energetically minimized computational modeling, together with MD simulation analysis revealed that subdomains 2 and 4 in LdACT are relatively closer than in muscle actin, which results in the reduced cleft volume and also generates additional direct interactions between Lys¹⁹ of LdACT with β - and γ -phosphates of ATP. Moreover, similar to muscle actin, Lys¹⁹ and Lys²¹⁴ showed hydrogen bonding with the sugar moiety of ATP, suggesting strong interactions of ATP with residues of the ATP binding cleft in LdACT and thus explaining the stronger ATPase activity of LdACT during polymerization. Alternatively, it may be due to the faster

Unconventional Actin in *Leishmania*

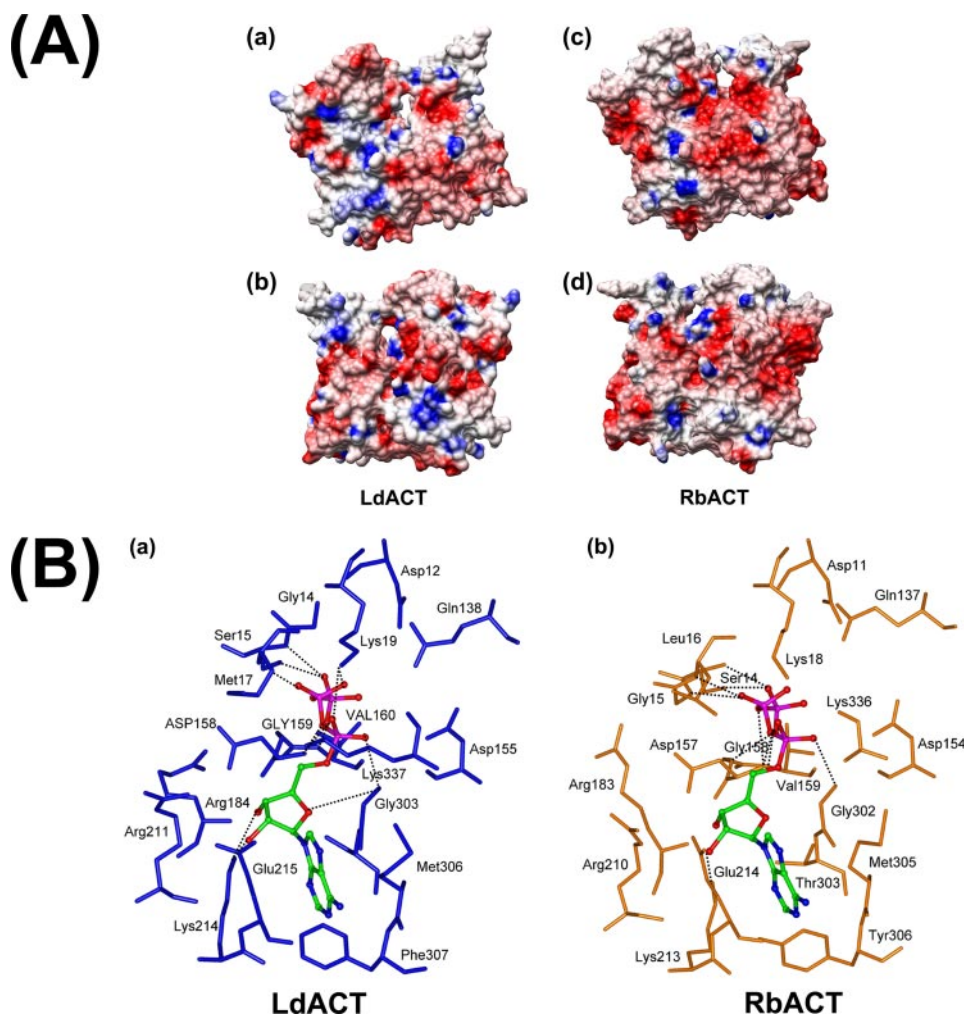


FIGURE 10. *A*, overall charge distribution on the surface of LdACT and RbACT. Solvent-exposed surface charges in red and blue represent positive and negative charges, respectively. *a–d* are the opposite faces of LdACT and RbACT, respectively. The molecular electrostatic potential was computed using GRASP program (69). *B*, ATP binding with LdACT and RbACT in the ATP binding cleft. *a* and *b* show hydrogen bonding interactions (dotted line) of ATP with the residues of LdACT and RbACT, respectively.

polymerization of rLdACT that like yeast actin could be due to the fragmentation of actin filaments, early during the polymerization, with the creation of more seeds (65). Moreover, P_i release during polymerization of LdACT was found to be faster than RbACT, which may be due to excessive treadmilling during the polymerization of LdACT suggesting high dynamics of LdACT filaments during the course of polymerization. Furthermore, the rate of ATP hydrolysis during rLdACT polymerization plateaus after $2 \mu\text{M}$ concentration, which could be attributed to the bundling property of rLdACT filaments beyond that concentration, leaving a large proportion of ATP-actin in the filaments. This further gains strength from the electron microscopic images of rLdACT filaments, which at $2 \mu\text{M}$ concentration, unlike RbACT, mainly existed as bundles. Interestingly, GTP binding with LdACT did not facilitate polymerization despite the presence of Phe³⁰⁷, which in the case of yeast actin has been shown to facilitate actin polymerization (66). This may be attributed to the orientation of the β - and γ -phosphate groups with respect to the heterocyclic ring that in the case of GTP may not be appropriate to facilitate additional interactions between these groups and Lys¹⁹ of LdACT.

residues that form the binding site (68) conserved in its structure, may be attributed to the overall structural differences between LdACT and conventional actins.

Based on these results, we conclude that LdACT is a novel form of actin that displays unique biochemical properties that have not been reported for any other actin to date. Finally, we suggest that LdACT could serve as an attractive target for designing novel antileishmanial drugs.

Acknowledgments—We express our gratitude to Dr. V. K. Bajpai (CDRI, Lucknow) and Dr. A. N. Ghosh (NICED, Kolkata) for consistent help in electron microscopy.

REFERENCES

1. Chang, K. P. (1983) *Int. Rev. Cytol. Suppl.* **14**, 267–305
2. Killick-Kendrick, R. (1990) *Ann. Parasitol. Hum. Comp.* **65**, 37–42
3. Balber, A. E. (1990) *Crit. Rev. Immunol.* **10**, 177–201
4. Webster, P., and Russell, D. G. (1993) *Parasitol. Today* **9**, 201–206
5. Engstler, M., Pfohl, T., Herminghaus, S., Boshart, M., Wiegertjes, G., Heddergott, N., and Overath, P. (2007) *Cell* **131**, 505–515
6. García-Salcedo, J. A., Pérez-Morga, D., Gijón, P., Dilbeck, V., Pays, E., and

- Nolan, D. P. (2004) *EMBO J.* **23**, 780–789
7. Reisler, E. (1993) *Curr. Opin. Cell Biol.* **3**, 41–47
8. Meza, I., Sabanero, M., Cazares, F., and Bryan, J. (1983) *J. Biol. Chem.* **258**, 3936–3941
9. Hirono, M., Kumagai, Y., Numata, O., and Watanabe, Y. (1989) *Proc. Natl. Acad. Sci. U. S. A.* **86**, 75–79
10. Mitchell, E. J., and Zimmerman, A. M. (1985) *J. Cell Sci.* **73**, 279–297
11. Sehring, I. M., Reiner, C., Mansfeld, J., Plattner, H., and Kissmehl, R. (2007) *J. Cell Sci.* **120**, 177–190
12. Uyemura, D. G., Brown, S. S., and Spudich, J. A. (1978) *J. Biol. Chem.* **253**, 9088–9096
13. Schmitz, S., Grainger, M., Howell, S., Calder, L. J., Gaeb, M., Pinder, J. C., Holder, A. A., and Veigel, C. (2005) *J. Mol. Biol.* **349**, 113–125
14. Schuler, H., Mueller, A. K., and Matuschewski, K. (2005) *FEBS Lett.* **579**, 655–660
15. Sahoo, N., Beatty, W., Heuser, J., Sept, D., and Sibley, L. D. (2006) *Mol. Biol. Cell* **17**, 895–906
16. Sahasrabudhe, A. A., Bajpai, V. K., and Gupta, C. M. (2004) *Mol. Biochem. Parasitol.* **134**, 105–114
17. Raza, S., Sahasrabudhe, A. A., and Gupta, C. M. (2007) *Mol. Biochem. Parasitol.* **153**, 216–219
18. Chen, M., and Shen, X. (2007) *Curr. Opin. Cell Biol.* **19**, 326–330
19. Mortara, R. A. (1989) *J. Protozool.* **36**, 8–13
20. Gull, K. (1999) *Annu. Rev. Microbiol.* **53**, 629–655
21. Hammarton, T. C., Wickstead, B., and Mc Kean, P. G. (2007) in *Trypanosomes: After The Genome* (Berry, D., Mottram, J., and Acosta-Serrano, A., ed) pp. 239–280, Wellcome Centre for Molecular Parasitology, University of Glasgow, Glasgow, UK
22. Shi, H., Djikeng, A., Mark, T., Wirtz, E., Tschudi, C., and Ullu, E. (2000) *RNA (Cold Spring Harbor)* **6**, 1069–1076
23. Nayak, R. C., Sahasrabudhe, A. A., Bajpai, V. K., and Gupta, C. M. (2005) *Mol. Biochem. Parasitol.* **143**, 152–164
24. Ozaki, L. S., and Cseko, Y. M. T. (1984) in *Genes and Antigens of Parasites, a Laboratory Manual* (Morel, C. M., ed) pp. 165–185, Fundacao Oswaldo Cruz, Rio de Janeiro
25. Sanger, F., Nicklen, S., and Coulson, A. R. (1977) *Proc. Natl. Acad. Sci. U. S. A.* **74**, 5463–5467
26. Ha, D. S., Schwarz, J. K., Turcob, S. J., and Beverley, S. M. (1996) *Mol. Biochem. Parasitol.* **77**, 57–64
27. Pardee, J. D., and Spudich, J. A. (1982) *Methods Enzymol.* **85**, 164–181
28. Pardee, J. D., and Spudich, J. A. (1982) *Methods Cell Biol.* **24**, 271–289
29. Ikkai, T., and Kondo, H. (2000) *IUBMB Life* **49**, 77–79
30. Frieden, C., Du, J., Schriefer, L., and Buzan, J. (2000) *Biochem. Biophys. Res. Commun.* **271**, 464–468
31. Wegner, A., and Engel, J. (1975) *Biophys. Chem.* **3**, 215–225
32. Blikstad, I., Markey, F., Carlsson, L., Persson, T., and Lindberg, U. (1978) *Cell* **15**, 935–943
33. Zeng, Z., Parmelee, D., Hyaw, H., Coleman, T. A., Su, K., Zhang, J., Gentz, R., Ruben, S., Rosen, C., and Li, Y. (1997) *Biochem. Biophys. Res. Commun.* **231**, 499–504
34. Geladopoulos, T. P., Sotiroudis, T. G., and Evangelopoulos, A. E. (1991) *Anal. Biochem.* **192**, 112–116
35. Thompson, J. D., Higgins, D. G., and Gibson, T. J. (1994) *Nucleic Acids Res.* **22**, 4673–4680
36. Felsenstein, J. (2004) *PHYMLIP* (Phylogeny Inference Package), Version 3.6b, University of Washington, Seattle, WA
37. Trooskens, G., De-Beule, D., Decouttere, F., and Van-Criekinge, W. (2005) *Bioinformatics* **21**, 3801–3802
38. Kudryashov, D. S., Sawaya, M. R., Adisetiyo, H., Norcross, T., Hegyi, G., Reisler, E., and Yeates, T. O. (2005) *Proc. Natl. Acad. Sci. U. S. A.* **102**, 13105–13110
39. Vorobiev, S., Strokopytov, B., Drubin, D. G., Frieden, C., Ono, S., Condeelis, J., Rubenstein, P. A., and Almo, S. C. (2003) *Proc. Natl. Acad. Sci. U. S. A.* **100**, 5760–5765
40. Accelrys Inc. (2000) *Insight II*, Accelrys Inc., San Diego, CA
41. Kabsch, W., Mannherz, H. G., Suck, D., Pai, E. F., and Holmes, K. C. (1990) *Nature* **347**, 37–44
42. Brooks, B. R., Brucoleri, R. E., Olafson, B. D., States, D. J., Swaminathan, S., and Karplus, M. (1983) *J. Comp. Chem.* **4**, 187–217
43. Ryckaert, J. P., Ciccitti, G., and Berendsen, H. J. C. (1977) *J. Comp. Phys.* **23**, 327–341
44. Humphrey, W., Dalke, A., and Schulten, K. (1996) *J. Mol. Graph.* **14**, 33–38
45. Esue, O., Cordero, M., Wirtz, D., and Tseng, Y. (2005) *J. Biol. Chem.* **280**, 2628–2635
46. Buzan, J., Du, J., Karpova, T., and Frieden, C. (1999) *Proc. Natl. Acad. Sci. U. S. A.* **96**, 2823–2827
47. Dean, W., Goddette, S., and Frieden, C. (1986) *J. Biol. Chem.* **261**, 15974–15980
48. Yarmola, E. G., Somasundaram, T., Boring, T. A., Spector, I., and Bubb, M. R. (2000) *J. Biol. Chem.* **275**, 28120–28127
49. Carlier, M. F., Pantaloni, D., Evans, J. A., Lambooy, P. K., Korn, E. D., and Webb, M. R. (1988) *FEBS Lett.* **235**, 211–214
50. Orlova, A., and Egelman, E. H. (1992) *J. Mol. Biol.* **227**, 1043–1053
51. Sheterline, P., and Sparrow, J. C. (1994) *Protein Profile* **1**, 1–121
52. Zheng, X., Diraviyam, K., and Sept, D. (2007) *Biophys. J.* **93**, 1277–1283
53. Martonosii, A., Molino, C. M., and Gergely, J. (1964) *J. Biol. Chem.* **239**, 1057–1064
54. Cooper, J. A., Buhle, E. L., Walker, J. B., Tsong, T. Y., and Pollard, T. D. (1983) *Biochemistry* **22**, 2193–2202
55. Carlier, M. F., Pantaloni, D., and Korn, E. D. (1986) *J. Biol. Chem.* **261**, 10778–10784
56. Rould, M. A., Wan, Q., Joel, P. B., Lowey, S., and Trybus, K. M. (2006) *J. Biol. Chem.* **281**, 31909–31919
57. Garner, E. C., Campbell, C. S., and Mullins, R. D. (2004) *Science* **306**, 1021–1025
58. Wang, F., Sampogna, R. V., and Ware, B. R. (1989) *Biophys. J.* **55**, 293–298
59. Glaser, T. A., Baatz, J. E., Kreishman, G. P., and Mukkada, A. J. (1988) *Proc. Natl. Acad. Sci. U. S. A.* **85**, 7602–7606
60. Holmes, K. C., Popp, D., Gebhard, W., and Kabsch, W. (1990) *Nature* **347**, 44–49
61. Galkin, V. E., VanLoock, M. S., Orlova, A., and Egelman, E. H. (2002) *Curr. Biol.* **12**, 570–575
62. Gheorghe, D. M., Aghamohammadzadeh, S., Smaczynska-de Rooij, I. I., Allwood, E. G., Winder, S. J., and Ayscough, K. R. (2008) *J. Biol. Chem.* **280**, 15037–15046
63. Yao, X., and Rubenstein, P. A. (2001) *J. Biol. Chem.* **276**, 25598–25604
64. Reisler, E., and Egelman, E. H. (2007) *J. Biol. Chem.* **282**, 36133–36137
65. Buzan, J. M., and Frieden, C. (1996) *Proc. Natl. Acad. Sci. U. S. A.* **93**, 91–95
66. Wen, K. K., Yao, X., and Rubenstein, P. A. (2002) *J. Biol. Chem.* **277**, 41101–41109
67. Drubin, D. G., Jones, H. D., and Wertman, K. F. (1993) *Mol. Biol. Cell* **4**, 1277–1294
68. Ahmed, S. A., Odde, S., Daga, P. R., Bowling, J. J., Mesbah, M. K., Youssef, D. T., Khalifa, S. I., Doerksen, R. J., and Hamann, M. T. (2007) *Org. Lett.* **9**, 4773–4776
69. Nicholls, A., Sharp, K. A., and Honig, B. (1991) *Proteins* **11**, 281–296